DYNAMIC RESPONSE OF THE HUMAN HEAD TO AN EXTERNAL STIMULUS

A. CHARALAMBOPOULOS, D.I. FOTIADIS
AND C.V. MASSALAS

12-98

Preprint no. 12-98/1998

Department of Computer Science
University of Ioannina
451 10 Ioannina, Greece

DYNAMIC RESPONSE OF THE HUMAN HEAD TO AN EXTERNAL STIMULUS

A. CHARALAMBOPOULOS
Polytechnic School, Mathematics Division, Aristotle University of Thessaloniki, GR 540 06 Thessaloniki, Greece

D.I. FOTIADIS
Dept. of Computer Science, University of Ioannina, GR 451 10 Ioannina Greece

and
C.V. MASSALAS*
Dept. of Mathematics, University of Ioannina, GR 451 10 Ioannina, Greece

SUMMARY

In this work we present an analysis concerning the mathematical formulation of the general problem of the dynamic loading of the human head. In the proposed analysis the system is assumed to constitute of a stratified spherical medium and a methodology is developed for the study of the dynamic behaviour of the human head. The response of the human head (displacement field and pressure) is investigated when a Dirac force in space and time is applied on it. The role of various parameters entering the dynamic characteristics of the system is extensively discussed.

* Author to whom correspondence should be addressed

1. INTRODUCTION

Several researchers have proposed models to study brain injuries due to external causes such as those resulting from car accidents. The human head - neck system is a very complicated structure and various geometrical and material approximations have been used in the modeling studies.

Among the earliest studies Goldsmith [1] provides an extensive review from the engineering and medical point of view. Liu [2] and King and Chou [3] presented survey articles on the mathematical modeling of head injuries. Advani and Owings [4] investigated the response of the a fluid - filled spherical shell. Shugar and Katona [5] have used finite element techniques to investigate the responses of spherical and plane strain head models giving particular emphasis on the determination of fluid pressure distribution and skull deflections. Akkas [6] analysed the dynamic response of a fluid - filled spherical shell using finite differences. Khalil and Hubbard [7] have studied the human head response to impact loading on three axisymmetric head model configurations using finite elements. Misra and Chakravarty [8] presented a model of the dynamic response of the human head - neck system, represented by a fluid - filled prolate spheroidal shell constrained by a viscoelastic beam.

Landkof and Goldsmith [9] performed an analytical and experimental study involving non-destructive, axisymmetric impact on a fluid - filled shell constrained by a viscoelastic artificial neck. Hickling and Wenner [10] developed a mathematical model using three - dimensional equations of linear viscoelasticity for the brain and the skull to predict the response of a human head to axisymmetric impact.

In previous communications we have extensively discussed the dynamic characteristics of the human head - neck system. We have studied simple systems [11-12] and more complicated ones which combine both geometry aspects [13-14] and material behavior of the brain and skull matter [15-16]. In Refs. 17 and 18 we have investigated the effect of the human neck support. In the above mentioned papers the role of the various parameters of the system on the dynamic characteristics (eigenfrequency and damping coefficients spectra, eigenfuctions) was investigated. The mathematical analysis was based on the expansion of the solution in terms of the Navier eigenvectors and the use of arguments from complex analysis and complicated numerical schemes.

In this work the system under consideration is assumed to constitute a stratified spherical medium. A number of models can be deduced from the general case, after making assumptions for the number of the spherical layers as well as their substance.

Consequently all the models simulating human brain system that have been adopted in previous works, can be studied under a stimulus state, in a uniform and deducible manner. More specifically, three models are described under stimulus state.

- the single elastic isotropic and homogeneous elastic skull
- the elastic skull filled with inviscid and irrotational fluid
- the two elastic spheres model

The methodology followed in the present work includes determination of the dynamic characteristics (eigenfrequencies and eigenvectors) for all the systems [11-18] and use of the proposed method to compute the displacement fields when a Dirac force in space and time is applied on it.

2. PROBLEM FORMULATION

The system under consideration is shown in Fig. 1 and consists of n spherical layers simulating the several regions of the human - brain system. According to the assumptions adopted in previous works concerning the physical characteristics of the several components of the system, every spherical layer of the model is assumed to be filled with an isotropic elastic material or with an inviscid and irrotational fluid of specific properties resembling the real situation. The exterior layer stands for the skull of the system and is considered, naturally, to be an elastic region. The well - posedness of the problem requires the satisfaction of suitable boundary conditions on the discontinuity surfaces of the system. As mentioned above the number and nature of the several components vary with the particular model under consideration and depend, of course, on the physical parameters whose involvement to the dynamic characteristics of the system, is studied in priority.

The main purpose of our analysis is the determination of the response of the system when a Dirac force, in space and time, is applied on it. More precisely, we suppose that the system is subjected to the external force $\boldsymbol{F}(\boldsymbol{r},t) = \boldsymbol{F}_o\delta(\boldsymbol{r}-\boldsymbol{r}_f)\delta(t)$, per unit mass, where $\boldsymbol{F}_o$ is an arbitrary vector, $\boldsymbol{r}_f$ is an arbitrary point of the region V_j and $\delta(\,)$ is the Dirac's δ - function. It is noticed here that response of the system to more general external forces can be deduced easily from the response to the Dirac force, which constitutes the Green function of the stimulus problem. In addition, the position vector $\boldsymbol{r}_f$ can be arbitrarily chosen, but its selection depends on the nature of the external force. Consequently, if we study the influence of the blood pressure due to cardiac pulses, $\boldsymbol{r}_f$ has to be selected near the central spherical region, but if we are

interested in responses to external stimuli, $\boldsymbol{r}_f$ must be placed very near the external surface S_n.

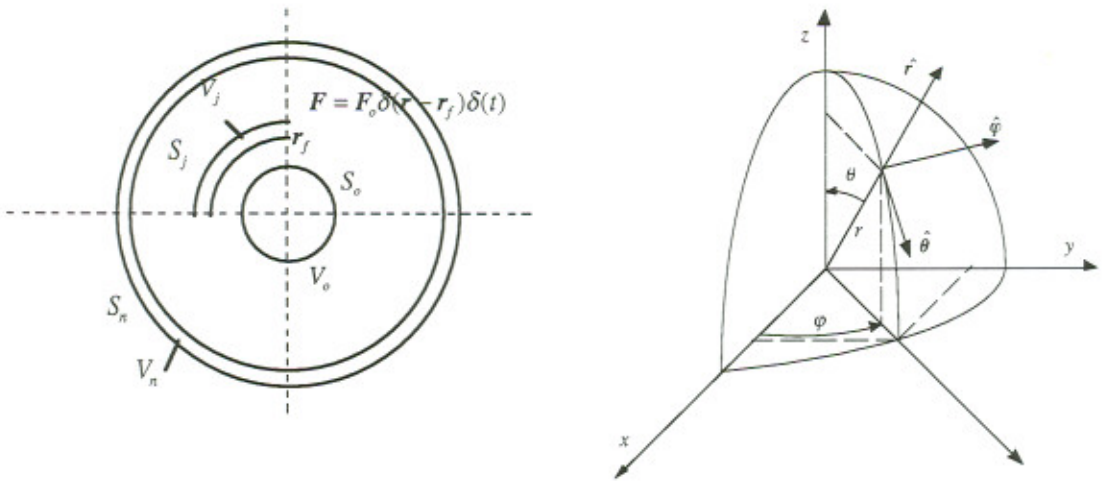

Figure 1: Problem Geometry and Coordinate System

In order to study the kinematic behavior of the system, we are going to determine the displacement field of every particular region.

More precisely, if the region V_i is an elastic one then the motion of this region is characterised by the displacement field $\boldsymbol{u}^{(i)}(\boldsymbol{r},t)$ satisfying the time - dependent non - homogeneous equation of elasticity,

$$\mu_i\nabla^2\boldsymbol{u}^{(i)}(\boldsymbol{r},t)+(\lambda_i+\mu_i)\nabla(\nabla\cdot\boldsymbol{u}^{(i)}(\boldsymbol{r},t))+\rho_i\delta^{(i,j)}\boldsymbol{F}_o\delta(\boldsymbol{r}-\boldsymbol{r}_f)\delta(t)=\rho_i\frac{\partial^2\boldsymbol{u}^{(i)}(\boldsymbol{r},t)}{\partial t^2} \qquad (1)$$

where μ_i, λ_i are Lamè's constants, ρ_i is the density of the region V_i and ∇ is the del operator. In addition $\delta^{(i,j)}$ is equal to 1 only if $i=j$ which means that $\boldsymbol{r}_f$ belongs to the region V_i, otherwise is equal to zero and repetition of a subscript does not mean summation with respect to it.

If the region V_i is occupied by an inviscid and irrotational fluid of density ρ_i and sound speed c_i, then the displacement field is obtained through the velocity potential satisfying

$$\nabla^2\Phi^{(i)}(\boldsymbol{r},t)=\frac{1}{c_i^2}\frac{\partial^2\Phi^{(i)}(\boldsymbol{r},t)}{\partial t}. \tag{2}$$

More precisely, the pressure and displacement fields are connected to the velocity potential through the equations

$$P^i(\boldsymbol{r},t)=-\rho_i\frac{\partial\Phi^{(i)}(\boldsymbol{r},t)}{\partial t} \tag{3}$$

$$\rho_i\ddot{\boldsymbol{u}}^{(i)}(\boldsymbol{r},t)=\rho_i\delta^{(i,j)}\boldsymbol{F}_o\delta(\boldsymbol{r}-\boldsymbol{r}_f)\delta(t)-\nabla P^{(i)}(\boldsymbol{r},t). \tag{4}$$

We apply Fourier transform analysis to the problem defining

$$\hat{\boldsymbol{u}}^{(i)}(\boldsymbol{r},\omega)=\int_{-\infty}^{+\infty}\boldsymbol{u}^{(i)}(\boldsymbol{r},t)e^{i\omega t}dt \tag{5}$$

$$\hat{\Phi}^{(i)}(\boldsymbol{r},\omega)=\int_{-\infty}^{+\infty}\Phi^{(i)}(\boldsymbol{r},t)e^{i\omega t}dt \tag{6}$$

$$\hat{P}^{(i)}(\boldsymbol{r},\omega)=\int_{-\infty}^{+\infty}P^{(i)}(\boldsymbol{r},t)e^{i\omega t}dt. \tag{7}$$

We suppress, for simplicity, the dependence of previously transformed functions on their argument ω and taking advantage of Fourier transform properties we get equations involving the transformed functions from the equations governing the initial fields.

For every elastic region V_i we obtain

$$\mu_i\nabla^2\hat{\boldsymbol{u}}^{(i)}(\boldsymbol{r})+(\lambda_i+\mu_i)\nabla(\nabla\cdot\hat{\boldsymbol{u}}^{(i)}(\boldsymbol{r}))+\rho_i\omega^2\hat{\boldsymbol{u}}^{(i)}(\boldsymbol{r})=-\rho_i\delta^{(i,j)}\boldsymbol{F}_o\delta(\boldsymbol{r}-\boldsymbol{r}_f), \tag{8}$$

while in any region V_i filled with fluid we obtain

$$\nabla^2\hat{\Phi}^{(i)}(\boldsymbol{r})+\frac{\omega^2}{c_i^2}\hat{\Phi}^{(i)}(\boldsymbol{r})=0 \tag{9}$$

$$\hat{P}^{(i)}(\boldsymbol{r}) = i\rho_i \omega \hat{\Phi}^{(i)}(\boldsymbol{r}) \tag{10}$$

$$\boldsymbol{u}^{(i)}(\boldsymbol{r}) = -\frac{1}{i\omega}\nabla\Phi^{(i)}(\boldsymbol{r}) - \frac{1}{\omega^2}\delta^{(i,j)}\boldsymbol{F}_o\delta(\boldsymbol{r}-\boldsymbol{r}_f). \tag{11}$$

Uniform handling of the several components of the system requires the introduction of dimensionless variables.

In this framework, the velocities $c_{p,i} = \sqrt{\frac{\lambda_i + 2\mu_i}{\rho_i}}$, $c_{s,i} = \sqrt{\frac{\mu_i}{\rho_i}}$ which characterise completely the elastic properties of the elastic medium V_i give place to $c'_{p,i} = \frac{c_{p,i}}{c_{p,n}}$, $c'_{s,i} = \frac{c_{s,i}}{c_{p,n}}$. Similarly, sound speed c_i in every fluid region V_i gives place to $c'_i = \frac{c_i}{c_{p,n}}$. In addition, the density ρ_i in every region V_i is replaced by the dimensionless density $\rho'_i = \frac{\rho_i}{\rho_n}$.

Finally, we define the dimensionless quantities

$$\boldsymbol{r}' = \frac{\boldsymbol{r}}{\alpha}, \quad \Omega = \frac{\omega\alpha}{c_{p,n}}, \quad \nabla' = \alpha\nabla, \quad (\alpha = r_n),$$

and the equations (8) - (11) in nondimensionalised form become

$$c'^2_{s,i}\nabla'^2\hat{\boldsymbol{u}}^{(i)}(\boldsymbol{r}') + (c'^2_{p,i} - c'^2_{s,i})\nabla'(\nabla'\cdot\hat{\boldsymbol{u}}^{(i)}(\boldsymbol{r}')) + \Omega^2\hat{\boldsymbol{u}}^{(i)}(\boldsymbol{r}') = -\delta^{(i,j)}\frac{\boldsymbol{F}_o\alpha}{c^2_{p,n}}\delta(\boldsymbol{r}' - \boldsymbol{r}'_f) \tag{12}$$

$$\nabla'^2\hat{\Phi}^{(i)}(\boldsymbol{r}') + \frac{\Omega^2}{c'^2_i}\hat{\Phi}^{(i)}(\boldsymbol{r}') = 0 \tag{13}$$

$$\hat{P}^{(i)}(\boldsymbol{r}') = i\Omega\rho'_i\frac{1}{c'^2_{s,n}}\hat{\Phi}^{(i)}(\boldsymbol{r}') \tag{14}$$

$$\hat{\boldsymbol{u}}^{(i)}(\boldsymbol{r}') = \frac{i}{\Omega}\nabla'\hat{\Phi}^{(i)}(\boldsymbol{r}') - \frac{\delta^{(i,j)}}{\Omega^2}\frac{\alpha}{c^2_{p,n}}\boldsymbol{F}_o\delta(\boldsymbol{r}' - \boldsymbol{r}'_f) \tag{15}$$

where $\hat{\Phi}^{(i)}(\boldsymbol{r}') \rightarrow "1"\hat{\Phi}^{(i)}(\boldsymbol{r}')$ is a dimensionless quantity and "1" has measure unity.

Applying ∇'^2 on equation (15) and using equation (13) we obtain

$$c'^2_i \nabla'^2 \hat{\boldsymbol{u}}^{(i)}(\boldsymbol{r}') + \Omega^2 \hat{\boldsymbol{u}}^{(i)}(\boldsymbol{r}') = -\delta^{(i,j)} \frac{\boldsymbol{F}_o \alpha}{c^2_{p,n}} \delta(\boldsymbol{r}' - \boldsymbol{r}'_f). \tag{16}$$

Comparing (12) and (16), we see that it is possible to express in an uniform way the equations governing the displacement fields $\hat{\boldsymbol{u}}^{(i)}(\boldsymbol{r}')$ after defining in a trivial manner, $c'_{p,i} = c'_{s,i} = c'_i$ in case where V_i is a region occupied by fluid.

Then

$$c'^2_{s,i} \nabla'^2 \hat{\boldsymbol{u}}^{(i)}(\boldsymbol{r}') + (c'^2_{p,i} - c'^2_{s,i}) \nabla' (\nabla' \cdot \hat{\boldsymbol{u}}^{(i)}(\boldsymbol{r}')) + \Omega^2 \hat{u}^{(i)}(\boldsymbol{r}') = -\delta^{(i,j)} \frac{\alpha}{c^2_{p,n}} \boldsymbol{F}_o \delta(\boldsymbol{r}' - \boldsymbol{r}'_f), \tag{17}$$

$\forall \; i = 0,1,2,...,n.$

Equations (17) must be accompanied by the suitable boundary conditions. More precisely, the exterior surface S_n is stress free, fact which is reflected in the condition $\boldsymbol{T}\hat{\boldsymbol{u}}_n(\boldsymbol{r}')\big|_{r'=\alpha} = \boldsymbol{0}$, where $\boldsymbol{T}$ is the surface traction operator [11].

Every surface S_i separating two elastic media must support equal displacement and stress fields from the two sides. In addition, every surface separating an elastic medium from a fluid filled one, must support equal displacement fields while the elastic stress field must be normal to the surface and compensate the fluid pressure. Finally two consecutive fluid regions apply to their discontinuity surface equal displacements and pressures.

Denoting uniformly

$$\left.\begin{aligned} \hat{\boldsymbol{u}}(\boldsymbol{r}') &= \hat{\boldsymbol{u}}^{(i)}(\boldsymbol{r}'), \text{ for } \boldsymbol{r}' \in V_i \\ c'_s(\boldsymbol{r}') &= c'_{s,i}, \text{ for } \boldsymbol{r}' \in V_i \\ c'_p(\boldsymbol{r}') &= c'_{p,i}, \text{ for } \boldsymbol{r}' \in V_i \end{aligned}\right\} \tag{18}$$

the equation governing the displacement field can be written through only one equation with non-constant coefficients, that is

$$c'_s(\boldsymbol{r}')^2\nabla'^2\hat{\boldsymbol{u}}(\boldsymbol{r}')+\left[c'_p(\boldsymbol{r}')^2-c'_s(\boldsymbol{r}')^2\right]\nabla'(\nabla'\cdot\hat{\boldsymbol{u}}(\boldsymbol{r}'))+\Omega^2\hat{\boldsymbol{u}}(\boldsymbol{r}')=-\frac{\boldsymbol{F}_o\alpha}{c_{p,n}^2}\delta(\boldsymbol{r}'-\boldsymbol{r}'_f),\ \ \boldsymbol{r}'\in V$$

.

(19)

Equation (19) accompanied with the above mentioned boundary conditions is a well - posed non-homogeneous boundary value problem.

Its solvability reduces to the corresponding homogeneous problem. More precisely, let us consider the boundary value problem consisting of the equation

$$c'_s(\boldsymbol{r}')^2\nabla'^2\hat{\varphi}(\boldsymbol{r}')+\left[c'_p(\boldsymbol{r}')^2-c'_s(\boldsymbol{r}')^2\right]\nabla'(\nabla'\cdot\hat{\varphi}(\boldsymbol{r}'))+\lambda^2\hat{\varphi}(\boldsymbol{r}')=0,\ \ \boldsymbol{r}'\in V \qquad (20)$$

and the same set of the boundary conditions satisfied by the solution of the non-homogeneous problem. But this is exactly the problem studied in previous works [11-18], which were referred to specific selections of geometrical and physical structures but all of them concerned the homogeneous boundary problem. Every model is provided with a sequence Ω_n^k of eigenvalues and a sequence of the corresponding eigenvectors $\hat{\boldsymbol{u}}_n^{m,k}(r')$, $\boldsymbol{r}'\in V$, $n=1,2,...;\ |\mathrm{m}|\le n;\ k=1,2,3,...$ where the pair (n,m) identifies the specific polar and azimuthal dependence of the eigenstate, while k enumerates the possible eigenstates belonging to the same state (n,m).

Generalised Sturm - Liouville theory guarantees that the set of functions $\hat{\boldsymbol{u}}_n^m(\boldsymbol{r}')$ constitutes a complete orthogonal set of functions in the space of square integrable functions in V. Orthogonality can be deduced by suitable application of Green's type theorem in space V, after using original Green's formulae for the fluid filled regions, Betti's formulae for the elastic ones and exploiting the boundary conditions satisfied by these solutions.

Orthogonality is expressed through the equation

$$\int\hat{\boldsymbol{u}}_n^{m,k}(\boldsymbol{r}')\cdot\hat{\boldsymbol{u}}_{n'}^{m',k'^*}(\boldsymbol{r}')d\boldsymbol{r}'=0,\ \ n\neq n'\ \ \text{or}\ m\neq m'\ \ \text{or}\ k\neq k'. \qquad (21)$$

Completeness of $\hat{\boldsymbol{u}}_n^{m,k}(\boldsymbol{r}')$ permits the following representation of the solution $\hat{\boldsymbol{u}}(\boldsymbol{r}')$ of the non-homogeneous problem

$$\hat{\boldsymbol{u}}(\boldsymbol{r}') = \sum_{n,m,k} \delta_n^{m,k}(\boldsymbol{r}'_f)\hat{\boldsymbol{u}}_n^{m,k}(\boldsymbol{r}'), \tag{22}$$

where summation extends over all possible values of indices n,m,k, $\delta_n^{m,k}(\boldsymbol{r}'_f)$ are the coefficients to be determined in order for $\hat{\boldsymbol{u}}(\boldsymbol{r}')$ to be found and of course these coefficients depend on the location of the impact.

Introducing (22) in (19), we find that

$$\sum_{n,m,k} \delta_n^{m,k}(\boldsymbol{r}'_f)(\Omega^2 - \Omega_n^{k2})\hat{\boldsymbol{u}}_n^{m,k}(\boldsymbol{r}') = -\frac{\boldsymbol{F}_o \alpha}{c_{p,n}^2}\delta(\boldsymbol{r}' - \boldsymbol{r}'_f). \tag{23}$$

Using the orthogonality of $\hat{\boldsymbol{u}}_n^{m,k}(\boldsymbol{r}')$ we obtain after projecting (23) on $\hat{\boldsymbol{u}}_n^{m,k}(\boldsymbol{r}')$ and integrating over V

$$\delta_n^{m,k}(\boldsymbol{r}'_f) = -\frac{\alpha \boldsymbol{F}_o \cdot \hat{\boldsymbol{u}}_n^{m,k^*}(\boldsymbol{r}'_f)}{c_{p,n}^2(\Omega^2 - \Omega_n^{k^2})} \frac{1}{\int_V \left|\hat{\boldsymbol{u}}_n^{m,k}(\boldsymbol{r}')\right|^2 d\boldsymbol{r}'}. \tag{24}$$

Denoting $\left\|\hat{\boldsymbol{u}}_n^{m,k}\right\| = \left(\int_V \left|\boldsymbol{u}_n^{m,k}(\boldsymbol{r}')\right|^2 d\boldsymbol{r}'\right)^{1/2}$, the norm of $\hat{\boldsymbol{u}}_n^{m,k}(\boldsymbol{r}')$ in the space of square integrable functions, we infer that equation (22) is written as

$$\hat{\boldsymbol{u}}(\boldsymbol{r}') = -\frac{\alpha \boldsymbol{F}_o}{c_{p,n}^2} \cdot \sum_{n,m,k} \frac{\hat{\boldsymbol{u}}_n^{m,k}(\boldsymbol{r}'_f)\hat{\boldsymbol{u}}_n^{m,k}(\boldsymbol{r}')}{(\Omega^2 - \Omega_n^{k2})\left\|\hat{\boldsymbol{u}}_n^{m,k}\right\|^2}. \tag{25}$$

We are now in position to determine $\boldsymbol{u}(\boldsymbol{r}',t)$ by taking the inverse Fourier transform of (25).

Consequently

$$\boldsymbol{u}(\boldsymbol{r}',t)=\frac{1}{2\pi}\int_{-\infty}^{+\infty}\hat{\boldsymbol{u}}(\boldsymbol{r}',\omega)e^{-i\omega t}d\omega=$$

$$=-\frac{1}{2\pi}\boldsymbol{F}_o\cdot\sum_{n,m,k}\hat{\boldsymbol{u}}_n^{m,k^*}(\boldsymbol{r}'_f)\hat{\boldsymbol{u}}_n^{m,k}(\boldsymbol{r}')\frac{1}{\left\|\hat{\boldsymbol{u}}_n^{m,k}\right\|^2}\int_{-\infty}^{+\infty}\frac{e^{-i\omega t}}{\omega^2-\omega_n^{k\,2}}d\omega \tag{26}$$

where $\omega_n^k=\frac{c_{p,n}}{\alpha}\Omega_n^k$.

Using complex analysis integration arguments, we finally obtain

$$\boldsymbol{u}(\boldsymbol{r}',t)=-\frac{i}{2}\boldsymbol{F}_o\cdot\sum_{n,m,k}\hat{\boldsymbol{u}}_n^{m,k^*}(\boldsymbol{r}'_f)\hat{\boldsymbol{u}}_n^{m,k}(\boldsymbol{r}')\frac{e^{i\omega_n^k t}}{\left\|\hat{\boldsymbol{u}}_n^{m,k}\right\|^2\omega_n^k}. \tag{27}$$

The explicit forms of $\hat{\boldsymbol{u}}_n^{m,k}(\boldsymbol{r}')$ in equation (27) are cited in the previous works [11-18], which refer to the determination of the dynamic characteristics of the corresponding systems.

As a matter of fact

$$\hat{\boldsymbol{u}}_n^{m,k}(\boldsymbol{r}')=\hat{\boldsymbol{u}}_{n,i}^{m,k}(\boldsymbol{r}')\ \text{for}\ \boldsymbol{r}'\in V_i \tag{28}$$

with

$$\hat{\boldsymbol{u}}_{n,i}^{m,k}(\boldsymbol{r}')=\sum_{l=1}^{2}\left\{\alpha_{n,i}^{m,l}\boldsymbol{L}_{n,i}^{m,l}(\boldsymbol{r}')+\beta_{n,i}^{m,l}\boldsymbol{M}_{n,i}^{m,l}(\boldsymbol{r}')+\gamma_{n,i}^{m,l}\boldsymbol{N}_{n,i}^{m,l}(\boldsymbol{r}')\right\}\Big|_{\Omega=\Omega_n^k}, \tag{29}$$

for V_i elastic, or

$$\hat{\boldsymbol{u}}_{n,i}^{m,k}(\boldsymbol{r}')=\frac{i}{c'_i}\sum_{l=1}^{2}c_{n,i}^{m,l}\boldsymbol{L}_{n,i}^{m,l}(\boldsymbol{r}')\Big|_{\Omega=\Omega_n^k} \tag{30}$$

for V_i filled with fluid.

In equations (29) and (30) the summation over l degenerates to only one term when the origin 0 belongs to V_i since in this case the spherical Bessel functions of second order must disappear [12].

We note that $\boldsymbol{L},\boldsymbol{M},\boldsymbol{N}$ stand for the Navier eigenvectors given by the relations

$$\begin{aligned}
\boldsymbol{L}_{n,i}^{m,l}(\boldsymbol{r}') &= \dot{g}_n^l(k'_{p,i}r')\boldsymbol{P}_n^m(\hat{\boldsymbol{r}}) + \sqrt{n(n+1)}\frac{g_n^l(k'_{p,i}r')}{k'_{p,i}r'}\boldsymbol{B}_n^m(\hat{\boldsymbol{r}}) \\
\boldsymbol{M}_{n,i}^{m,l}(\hat{\boldsymbol{r}}) &= \sqrt{n(n+1)}g_n^l(k'_{s,i}r')\boldsymbol{C}_n^m(\hat{\boldsymbol{r}}) \\
\boldsymbol{N}_{n,i}^{m,l}(\boldsymbol{r}') &= n(n+1)\frac{g_n^l(k'_{s,i}r')}{k'_{s,i}r'}\boldsymbol{P}_n^m(\hat{\boldsymbol{r}}) + \sqrt{n(n+1)}\left\{\dot{g}_n^l(k'_{s,i}r') + \frac{g_n^l(k'_{s,i}r')}{k'_{s,i}r'}\right\}\boldsymbol{B}_n^m(\hat{\boldsymbol{r}})
\end{aligned} \tag{31}$$

where $\dot{g}_n^l(z)$ stands for the derivative of the spherical Bessel $g_n^l(z)$ ($j_n(z)$ for $l=1$ and $y_n(z)$ for $l=2$) with respect to its argument and the functions $\boldsymbol{P}_n^m(\hat{\boldsymbol{r}}),\boldsymbol{B}_n^m(\hat{\boldsymbol{r}}),\boldsymbol{C}_n^m(\hat{\boldsymbol{r}})$ constitute the vector spherical harmonics given by

$$\begin{aligned}
\boldsymbol{P}_n^m(\hat{\boldsymbol{r}}) &= \hat{\boldsymbol{r}}Y_n^m(\hat{\boldsymbol{r}}) \\
\boldsymbol{B}_n^m(\hat{\boldsymbol{r}}) &= \frac{1}{\sqrt{n(n+1)}}\left\{\hat{\vartheta}\frac{\partial}{\partial\vartheta} + \hat{\varphi}\frac{1}{\sin\vartheta}\frac{\partial}{\partial\varphi}\right\}Y_n^m(\hat{\boldsymbol{r}}) \\
\boldsymbol{C}_n^m(\hat{\boldsymbol{r}}) &= \frac{1}{\sqrt{n(n+1)}}\left\{\hat{\vartheta}\frac{1}{\sin\vartheta}\frac{\partial}{\partial\varphi} - \hat{\varphi}\frac{\partial}{\partial\vartheta}\right\}Y_n^m(\hat{\boldsymbol{r}})
\end{aligned}$$

where $\hat{\boldsymbol{r}},\hat{\vartheta},\hat{\varphi}$ are the unit vectors in the r,ϑ,φ - directions respectively and $Y_n^m(\hat{\boldsymbol{r}})$ the spherical harmonics. Finally k' stands for the dimensionless wave numbers, i.e., $k'_{p,i}=\dfrac{\Omega}{c'_{p,i}}$, $k'_{s,i}=\dfrac{\Omega}{c'_{s,i}}$.

The coefficients $\alpha,\beta,\gamma,\delta$ are determined modulo a multiplicative constant - as coefficients of eigenvectors - but this does not alter the expression (27) because as easily can be proved the homogeneous way $\hat{\boldsymbol{u}}_n^{m,k}$ enters (27) cancels this multiplicative constant.

What remains to be calculated is the norm $\left\|\hat{\boldsymbol{u}}_n^{m,k}\right\|$ appearing in (27).

Clearly,

$$\left\|\hat{\boldsymbol{u}}_n^{m,k}\right\|^2 = \int_V \hat{\boldsymbol{u}}_n^{m,k}(\boldsymbol{r}') \cdot \hat{\boldsymbol{u}}_n^{m,k^*}(\boldsymbol{r}')d\boldsymbol{r}' = \sum_{i=0}^{n} \int_{V_i} \hat{\boldsymbol{u}}_{n,i}^{m,k}(\boldsymbol{r}') \cdot \hat{\boldsymbol{u}}_{n,i}^{m,k^*}(\boldsymbol{r}')d\boldsymbol{r}' . \tag{32}$$

We have then to determine every particular term $\int_{V_i} \hat{\boldsymbol{u}}_{n,i}^{m,k}(\boldsymbol{r}') \cdot \hat{\boldsymbol{u}}_{n,i}^{m,k^*}(\boldsymbol{r}')d\boldsymbol{r}'$.

First Case: V_i - elastic region

Inserting expression (29) in the integral and using orthogonality arguments for the Navier eigenvectors, we find that

$$\int_{V_i} \hat{\boldsymbol{u}}_{n,i}^{m,k}(\boldsymbol{r}') \cdot \hat{\boldsymbol{u}}_{n,i}^{m,k^*}(\boldsymbol{r}')d\boldsymbol{r}' = \sum_{l=1}^{2} \left\{ \begin{array}{l} \left|\alpha_{n,i}^{m,l}\right|^2 \left\|\boldsymbol{L}_{n,i}^{m,l}(\boldsymbol{r}')\right\|^2 + \left|\beta_{n,i}^{m,l}\right|^2 \left\|\boldsymbol{M}_{n,i}^{m,l}(\boldsymbol{r}')\right\|^2 + \left|\gamma_{n,i}^{m,l}\right|^2 \left\|\boldsymbol{N}_{n,i}^{m,l}(\boldsymbol{r}')\right\|^2 \\ +2\,\mathrm{Re}\left\{ \alpha_{n,i}^{m,l} \gamma_{n,i}^{m,l^*} \int_{V_i} \boldsymbol{L}_{n,i}^{m,l}(\boldsymbol{r}') \cdot \boldsymbol{N}_{n,i}^{m,l^*}(\boldsymbol{r}')d\boldsymbol{r}' \right\} \end{array} \right\}_{\Omega=\Omega_n^k} \tag{33}$$

where $\left\|\boldsymbol{L}_{n,i}^{m,l}(\boldsymbol{r}')\right\|$, $\left\|\boldsymbol{M}_{n,i}^{m,l}(\boldsymbol{r}')\right\|$, $\left\|\boldsymbol{N}_{n,i}^{m,l}(\boldsymbol{r}')\right\|$ stand for the L^2 - norms of the corresponding functions in space V_i. Expression (33) is obtained after determining the above mentioned norms and the last integral expressing the inner product of $\boldsymbol{L}_{n,i}^{m,l}$ and $\boldsymbol{N}_{n,i}^{m,l}$. The explicit form of the Navier eigenvectors given in equation (31) indicate that the determination of these norms is a rather difficult task. As a matter of fact, the polar and azimuthal integrations are handled in a straightforward manner, by exploiting orthogonality of spherical harmonic functions. In contrast, the radial integrals have complicated form and was needed tedious and elaborate techniques based on properties of spherical Bessel functions in order to avoid numerical integration and to express all the results in a closed analytical form. We considered this effort necessary in order not to aggravate the problem with numerical error which is controlled with difficulty when someone has to deal with spherical Bessel functions of second order. The expressions for the above quantities are given in Appendix A.

Second Case: V_i - fluid region

In this case, equation (30) leads immediately to the result

$$\int_{V_i} \hat{\boldsymbol{u}}_{n,i}^{m,k}(\boldsymbol{r}') \cdot \hat{\boldsymbol{u}}_{n,i}^{m,k^*}(\boldsymbol{r}')\, d\boldsymbol{r}' = \frac{1}{c_i'^2} \left| c_{n,i}^{m} \right|^2 \left\| \boldsymbol{L}_{n,i}^{m,l} \right\|^2 \Big|_{\Omega=\Omega_n^k} \tag{34}$$

and clearly suffices only knowledge of the norm $\left\| \boldsymbol{L}_{n,i}^{m,l} \right\|$ to determine the investigated integral.

3. NUMERICAL RESULTS

For each model the following algorithm is followed:

1. Solve the corresponding homogeneous problem and find Ω_n^k and the corresponding vector of coefficients $\boldsymbol{x}$ from the frequency equation shown in Appendix C for each model.
2. Use of a quicksort [19] algorithm to order Ω_n^k in ascending order.
3. Use equation (27) to compute the displacement fields under the state of an external Dirac force $\boldsymbol{F}_0$.

The frequency equation for each model is solved numerically using a bisection method for Ω_n^k, $n = 1,2,3,...;\ k = 1,2,3,....$ A singular value decomposition is used for the determination of each corresponding eigenvector. Those eigenfrequencies are ordered in ascending order using a quicksort algorithm. Equation (27) is used for the computation of the displacement field. An iterative procedure is followed and the number k' of the eigenfrequencies (and eigenvectors) used and this procedure terminates when $\left\| \boldsymbol{u}(\boldsymbol{r}',t)^{(k')} - \boldsymbol{u}(\boldsymbol{r}',t)^{(k'+1)} \right\| \approx O\left(10^{-8}\right)$. An example of the numerical results obtained for the FF - Model is shown in Fig. 1 for $k' = 21,41,51$ for u_r. It is noted that in our computation the accuracy of the bisection method used is of the order of $O\left(10^{-8}\right)$ and that the value of k' for convergence is strongly dependent on the model under discussion.

In what follows we present numerical results for the models considered under the influence of the external stimulus

$$\boldsymbol{F}_0 = (F_{0_r}, F_{0_\theta}, F_{0_\varphi}) = (1,0,0)$$

applied on

$\boldsymbol{r}_f = (r_{f_r}, r_{f_\theta}, r_{f\varphi}) = (1.0, 0, 0)$.

Dry Skull (S - Model)

The material properties used are analogous to those of Ref. 21:

$E = 1.379 \times 10^9 N/m^2,\ \nu = 0.25,\ \rho = 2.132 \times 10^3 kg/m^3$
$r_1 = 0.082m,\ r_0 = 0.076m$

The frequency equation matrix is given in Appendix C.1 and its size is 6 X 6 [11]. The value of k' used in our computations is 35 and we have computed 45 eigenfrequencies for $0 \le n \le 20$ and $0.0 \le \Omega_n^k \le 10.0$. The results obtained for the displacement fields are shown in Figs. 3 and 4 as a function of time for $\theta = 0$ and $\theta = \pi/2$, respectively. The time scale displayed corresponds to $0 \le t \le 1000\ \mu$sec and in the enclosed framed figure this is extended up to 500 μsec. The corresponding displacement fields as function of $0 \le \varphi \le 2\pi$ for discrete time steps are shown in Fig. 5.

Two Elastic Spheres (EE - Model)

The material properties used are similar to those used in Ref. 12:
$E_1 = 6.5 \times 10^9 N/m^2,\ \nu_1 = 0.25,\ \rho_1 = 2.132 \times 10^3 kg/m^3$
$E_0 = ...N/m^2,\ \nu_0 = 0.48,\ \rho_0 = 1.0002 \times 10^3 kg/m^3$
$r_1 = 0.082m,\ r_0 = 0.076m$

The frequency equation matrix is given in Appendix C.2 and its size is 9 X 9 [12]. The value of k' used in our computations is 85 and we have computed 660 eigenfrequencies for $0 \le n \le 25$ and $0.0 \le \Omega_n^k \le 10.0$. The results obtained for the displacement fields are shown in Figs. 6 and 7 as a function of time for $\theta = 0$ and $\theta = \pi/2$, respectively. The time scale displayed corresponds to $0 \le t \le 1000\ \mu$sec and in the enclosed framed figure this is extended up to 500 μsec. The corresponding displacement fields as function of $0 \le \varphi \le 2\pi$ for discrete time steps are shown in Fig. 8.

Elastic Skull Filled with Fluid (FF - Model)

The material properties used are similar to those used in Ref. 12:

$E_1 = 6.5\times10^9\, N/m^2,\ \nu_1 = 0.25,\ \rho_1 = 2.132\times10^3\, kg/m^3$

$K = 2.1029753\times10^9\, N/m^2,\ \rho_f = 1.0002\times10^3\, kg/m^3$

$r_1 = 0.082m,\ r_0 = 0.076m$

The frequency equation matrix is given in Appendix C.3 and its size is 7 X 7 [12]. The value of k' used in our computations is 51 and we have computed 88 eigenfrequencies for $0 \le n \le 25$ and $0.0 \le \Omega_n^k \le 10.0$. The results obtained for the displacement fields are shown in Figs. 9 and 10 as a function of time for $\theta = 0$ and $\theta = \pi/2$, respectively. The time scale displayed corresponds to $0 \le t \le 100\ \mu$sec and in the enclosed framed figure this is extended up to 500 μsec. The corresponding displacement fields as function of $0 \le \varphi \le 2\pi$ for discrete time steps are shown in Fig. 11.

The determination of pressure distribution in the fluid requires special treatment as it is shown below.

From equation (15) follows that

$$\nabla' \cdot \hat{\boldsymbol{u}}^{(i)}(\boldsymbol{r}') = \frac{i}{\Omega}\nabla'^2\,\hat{\Phi}^{(i)}(\boldsymbol{r}'),\ \text{for}\ \boldsymbol{r}' \neq r'_f \tag{35}$$

and combining equations (13), (14) and (35) we obtain

$$\hat{P}^{(i)} = -i\Omega\rho'_i \frac{1}{c'^2_{s,n}}\frac{c'^2_i}{\Omega^2}\nabla'^2\,\hat{\Phi}^{(i)} = -\rho'_i \frac{1}{c'^2_{s,n}} c'^2_i\,(\nabla' \cdot \hat{\boldsymbol{u}}^{(i)}). \tag{36}$$

However according to (25)

$$\nabla' \cdot \hat{\boldsymbol{u}}^{(i)}(\boldsymbol{r}') = -\frac{\alpha}{c'^2_{p,n}} \sum_{n,m,k} \frac{(F_0 \cdot \hat{\boldsymbol{u}}_n^{m,k}(\boldsymbol{r}'_f))\left(\nabla' \cdot \hat{\boldsymbol{u}}_{n,i}^{m,k}(\boldsymbol{r}')\right)}{\left(\Omega^2 - \Omega_n^{k2}\right)\left\|\hat{\boldsymbol{u}}_n^{m,k}\right\|^2}. \tag{37}$$

Given that the i region is a fluid

$$\hat{\boldsymbol{u}}_{n,i}^{m,k}(\boldsymbol{r}') = \frac{i}{c'_i}\sum_{l=1}^{2} c_{n,i}^{m,l}\boldsymbol{L}_{n,i}^{m,l}(\boldsymbol{r}')\Big|_{\Omega=\Omega_n^k} = \frac{i}{c'_i}\sum_{l=1}^{2} c_{n,i}^{m,l}\nabla'\Psi_{n,i}^{m,l}(\boldsymbol{r}')\Big|_{\Omega=\Omega_n^k} \tag{38}$$

where $\Psi_{n,i}^{m,l} = g_n^l(k'_{p,i}r')Y_n^m(\hat{\boldsymbol{r}})$.

Combining (38) with (37) we obtain

$$\nabla'\cdot\hat{\boldsymbol{u}}^{(i)}(\boldsymbol{r}') = \frac{i\alpha}{c'_i c'^2_{p,n}}\sum_{n,m,k}\frac{\boldsymbol{F}_0\cdot\hat{u}_n^{m,k}(\boldsymbol{r}'_f)}{\left(\Omega^2-\Omega_n^{k\,2}\right)}\frac{k'_{p,i}}{\left\|\hat{\boldsymbol{u}}_n^{m,k}\right\|^2}\left[\sum_{l=1}^{2} c_{n,i}^{m,l}g_n^l(k'_{p,i}r')Y_n^m(\hat{\boldsymbol{r}})\right]$$

or

$$P^{(i)}(\boldsymbol{r},t) = -\frac{i\alpha c'_i}{c'^2_{p,n}c'^2_{s,n}}\sum_{n,m,k}\frac{\boldsymbol{F}_0\cdot\hat{u}_n^{m,k}(\boldsymbol{r}'_f)}{\left(\Omega^2-\Omega_n^{k\,2}\right)}\frac{k'_{p,i}}{\left\|\hat{\boldsymbol{u}}_n^{m,k}\right\|^2}\left[\sum_{l=1}^{2} c_{n,i}^{m,l}g_n^l\left(\frac{\Omega_n^k}{c'_{p,i}}r'\right)Y_n^m(\hat{\boldsymbol{r}})\right]$$

and taking the inverse transform we finally obtain that

$$P^{(i)}(\boldsymbol{r},t) = \frac{\rho'_i c'_i}{2\alpha c'^2_{s,n}}\sum_{n,m,k}\frac{\boldsymbol{F}_0\cdot\hat{u}_n^{m,k}(\boldsymbol{r}'_f)e^{i\omega_n^k t}}{\omega_n^k}\frac{k'_{p,i}}{\left\|\hat{\boldsymbol{u}}_n^{m,k}\right\|^2}\left[\sum_{l=1}^{2} c_{n,i}^{m,l}g_n^l\left(\frac{\Omega_n^k}{c'_{p,i}}r'\right)Y_n^m(\hat{\boldsymbol{r}})\right].$$

The pressure variation is shown in Figs. 12 and 13 as a function of time and space respectively.

4. CONCLUSIONS

We have presented a general approach to the dynamic loading of the human head. The method is based on the solution of the corresponding homogeneous system for its eigenfrequencies and eigenvectors and computation of the displacement fields when a Dirac force in space and time is applied on it. The methodology has been developed for the spherical geometry and the various components of the human head are represented as spherical layers. The exterior layer stands for the skull and the other ones for brain and cerebrospinal fluid. We have used three models to investigate the response of the human head and those include the simple human skull, the fluid filled human skull and the elastic filled human skull. The method can easily be extended to other geometries and to other material properties. The displacement fields presented in this work can be used for the observation of the human head response in various conditions which

involve external cause, such as car accidents or blows in boxing. This can also be used for the computation of intracranial pressure and its variations to estimate sudden increase which becomes very critical and sometimes cause of death.

Acknowledgment
The present work forms part of the project "New Systems for Early Medical Diagnosis and Biotechnological Applications" which is supported by the Greek General Secretariat for Research and Technology through the EU funded R & D Program EPET II.

References

[1] Goldsmith, W. (1970) Biomechanics of Head Injury. In Biomechanics: Its Foundations and Objectives. (Edited by Fung, Y.C., Perrone N., and Anliker, M.), Prentice Hall, Englewood Cliffs, NJ.

[2] Liu, Y.K., (1970) The Biomechanics of Spinal and Head Impact: Problems of Mathematical Simulation. Proc. Symp. Biodynamic Modeling and its Applications, pp 701-736, Dayton, OH.

[3] King, A.I. and Chou C.C. (1975) Mathematical Modeling, Simulation and Experimental Testing of Biomechanical System Crash Response. AIAA Paper No. 75 - 272.

[4] Advani, S.H. and Owings, R.P. (1975) Structural Modeling of Human Head. ASCE, J. Engng. Mech. Div. 3 pp 257-266.

[5] Shugar, T.A. and Katona M.G. (1975) Development of Finite Element Head Injury Model. ASCE J. Engng. Mech. Div. EM3, pp. 223-239.

[6] Akkas, N. (1975) Dynamic Analysis of a Fluid - Filled Spherical Sandwich Shell - a Model of the Human Head. J. Biomechanics, 8, 275-284.

[7] Khalil, T.B. and Hubbard R.P. (1977) Parametric Study of Head Response by Finite Element Modelling. J. Biomechanics 10 119-132.

[8] Misra J.C., and Chakravarty S.(1985) Dynamic Response of a Head - Neck System to an Impulsive Load. Mathematical Modelling 6 83-96.

[9] Landkof, B., Goldsmith W., and Sackman J.L. (1976) Impact on a Head - Neck Structure. J. Biomechanics 9 141-151.

[10] Hickling, R. and Wenner, M.L. (1973) Mathematical Model of a Head Subjected to an Axisymmetric Impact. J. Biomechanics 6 115-132.

[11] Charalampopoulos, A., Dassios, G., Fotiadis, D.I., Kostopoulos, V., and Massalas, C.V. (1996) On the Dynamic Characteristics of the Human Skull. Int. J. Engng. Sci. 34(12) 1339-1348.

[12] Charalambopoulos, A., Dassios, G., Fotiadis, D.I., and Massalas, C.V. (1998) Dynamic Characteristics of the Human Skull - Brain System. Computer and Mathematical Modelling 27(2) 81-101.

[13] Charalambopoulos, A., Fotiadis, D.I., and Massalas, C.V. (1998) Free Vibrations of the Viscoelastic Human Skull. Int. J. Engng. Sci. (to appear).

[14] Charalambopoulos, A., Fotiadis, D.I., and Massalas, C.V. (1998) The Effect of Viscoelastic Brain on the Dynamic Characteristics of the Human Skull - Brain System. Acta Mechanica (to appear).

[15] Charalambopoulos, A., Fotiadis, D.I., and Massalas, C.V. (1998) The Effect of Geometry on the Dynamic Characteristics of the Human Skull. Int. J. Engng. Sci. (to appear).

[16] Charalambopoulos, A., Fotiadis, D.I., and Massalas, C.V. (1998) Frequency Spectrum of the Bispherical Hollow System: The Case of the Nonuniform Thickness Human Skull. Acta Mechanica (to appear).

[17] Charalambopoulos, A., Dassios, G., Fotiadis, D.I., and Massalas, C.V. (1997) Frequency Spectrum of the Human Head - Neck System, Int. J. Engng. Sci. 35(8)753-768.

[18] Charalambopoulos, A., Fotiadis, D.I., and Massalas, C.V. (1998) Human Head - Neck System: The Effect of Viscoelastic Neck on the Eigenfrequency Spectrum. Applied Mechanics (submitted).

[19] Press, W.H., Teukolsky, S.A., Vetterling, W.T., and Flannery, B.P. (1992) Numerical Recipes in FORTRAN: The Art of Scientific Computing, 2nd Edition. Cambridge University Press, Cambridge.

[20] Zhang, S. and Jin, J. (1996) Computation of Special Functions. John Wiley Interscience.

[21] McElhaney J.H. (1970) Mechanical Properties of cranial bone, J. Biomechanics 3 495-511.

APPENDIX A

$$\left\|\boldsymbol{L}_{n,i}^{m,l}\right\|^2 = \frac{1}{k'_{p,i}}\left[r'^2\, g_n^l(k'_{p,i}r')\dot{g}_n^l(k'_{p,i}r')\right]_{\alpha'_{i-1}}^{\alpha'_i} + A^p(\alpha'_{i-1},\alpha'_i)$$

$$\left\|\boldsymbol{M}_{n,i}^{m,l}\right\|^2 = n(n+1)A^s(\alpha'_{i-1},\alpha'_i)$$

$$\left\|\boldsymbol{N}_{n,i}^{m,l}\right\|^2 = \frac{1}{k'_{s,i}}\left[r'^2\, g_n^l(k'_{s,i}r')\dot{g}_n^l(k'_{s,i}r')\right]_{\alpha'_{i-1}}^{\alpha'_i} - \left[n(n+1)+2\right]A^s(\alpha'_{i-1},\alpha'_i) +$$

$$+\frac{1}{k'_{s,i}}\left[r'^3\,\dot{g}_n^l(k'_{s,i}r')\left[\left(\frac{n(n+1)}{r'}-k'_{s,i}r'\right)g_n^l(k'_{s,i}r') - k'_{s,i}\,\dot{g}_n^l(k'_{s,i}r')\right]\right]_{\alpha'_{i-1}}^{\alpha'_i}$$

$$+3\left[r'^3\,(g_n^l(k'_{s,i}r'))^2\right]_{\alpha'_{i-1}}^{\alpha'_i} - k'_{s,i}\left[r'^3\,\dot{g}_n^l(k'_{s,i}r')g_n^l(k'_{s,i}r')\right]_{\alpha'_{i-1}}^{\alpha'_i}$$

$$+2\left[r'^3\left(\dot{g}_n^l(k'_{s,i}r')\right)^2\right]_{\alpha'_{i-1}}^{\alpha'_i}$$

$$\int_{V_i}\boldsymbol{L}_{n,i}^{m,l}\cdot\boldsymbol{N}_{n,i}^{m,l*} = \frac{n(n+1)}{k'_{s,i}k'_{p,i}}\left[r'\,g_n^l(k'_{s,i}r')g_n^l(k'_{p,i}r')\right]_{\alpha'_{i-1}}^{\alpha'_i}$$

where

$$A^s(\alpha'_{i-1},\alpha'_i)$$

$$= \frac{\pi}{4k'^3_{s,i}}\left[k'^2_{s,i}r'^2\left[\dot{G}^l_{n+\frac{1}{2}}(k'_{s,i}r')\right]^2 - \left(n+\frac{1}{2}\right)\left[G^l_{n+\frac{1}{2}}(k'_{s,i}r')\right]^2 + k'^2_{s,i}r'^2\left[G^l_{n+\frac{1}{2}}(k'_{s,i}r')\right]^2\right]_{\alpha'_{i-1}}^{\alpha'_i}$$

$$A^p(\alpha'_{i-1},\alpha'_i)$$

$$= \frac{\pi}{4k'^3_{p,i}}\left[k'^2_{p,i}r'^2\left[\dot{G}^l_{n+\frac{1}{2}}(k'_{p,i}r')\right]^2 - \left(n+\frac{1}{2}\right)\left[G^l_{n+\frac{1}{2}}(k'_{p,i}r')\right]^2 + k'^2_{p,i}r'^2\left[G^l_{n+\frac{1}{2}}(k'_{p,i}r')\right]^2\right]_{\alpha'_{i-1}}^{\alpha'_i}$$

and

$$[f]_\alpha^\beta = f(\beta) - f(\alpha).$$

APPENDIX B

All systems above result to the following set of equations

$$\boldsymbol{Dx} = \boldsymbol{0}, \quad \boldsymbol{D} = \left[d_{i,j} \right].$$

Case 1: Elastic Sphere Model (Only Skull)

$$\begin{bmatrix} A_n^1(r'_1) & A_n^2(r'_1) & 0 & 0 & D_n^1(r'_1) & D_n^2(r'_1) \\ B_n^1(r'_1) & B_n^2(r'_1) & 0 & 0 & E_n^1(r'_1) & E_n^2(r'_1) \\ 0 & 0 & C_n^1(r'_1) & C_n^2(r'_1) & 0 & 0 \\ A_n^1(r'_0) & A_n^2(r'_0) & 0 & 0 & D_n^1(r'_0) & D_n^2(r'_0) \\ B_n^1(r'_0) & B_n^2(r'_0) & 0 & 0 & E_n^1(r'_0) & E_n^2(r'_0) \\ 0 & 0 & C_n^1(r'_0) & C_n^2(r'_0) & 0 & 0 \end{bmatrix} \begin{bmatrix} \alpha_n^{m,1} \\ \alpha_n^{m,2} \\ \beta_n^{m,1} \\ \beta_n^{m,2} \\ \gamma_n^{m,1} \\ \gamma_n^{m,2} \end{bmatrix} = \boldsymbol{0}$$

Case 2: Fluid Filled Elastic Sphere

$$\begin{bmatrix} A_n^1(r'_1) & A_n^2(r'_1) & 0 & 0 & D_n^1(r'_1) & D_n^2(r'_1) & 0 \\ B_n^1(r'_1) & B_n^2(r'_1) & 0 & 0 & E_n^1(r'_1) & E_n^2(r'_1) & 0 \\ 0 & 0 & C_n^1(r'_1) & C_n^2(r'_1) & 0 & 0 & 0 \\ A_n^1(r'_0) & A_n^2(r'_0) & 0 & 0 & D_n^1(r'_0) & D_n^2(r'_0) & d_{4,7} \\ B_n^1(r'_0) & B_n^2(r'_0) & 0 & 0 & E_n^1(r'_0) & E_n^2(r'_0) & 0 \\ 0 & 0 & C_n^1(r'_0) & C_n^2(r'_0) & 0 & 0 & 0 \\ d_{7,1} & d_{7,2} & 0 & 0 & d_{7,5} & d_{7,6} & d_{7,7} \end{bmatrix} \begin{bmatrix} \alpha_n^{m,1} \\ \alpha_n^{m,2} \\ \beta_n^{m,1} \\ \beta_n^{m,2} \\ \gamma_n^{m,1} \\ \gamma_n^{m,2} \\ c_{nm} \end{bmatrix} = \boldsymbol{0}$$

where

$$d_{4,7} = i\Omega \frac{\rho'_f}{c'^2_s} g_n^1(k'_f r'_0), \quad d_{7,1} = \dot{g}_n^1(\Omega r'_0), \quad d_{7,2} = \dot{g}_n^2(\Omega r'_0),$$

$$d_{7,5} = n(n+1) \frac{g_n^1(k'_s r'_0)}{k'_s r'_0}, \quad d_{7,6} = n(n+1) \frac{g_n^2(k'_s r'_0)}{k'_s r'_0}, \quad d_{7,7} = -\frac{i}{c'_f} \dot{g}_n^1(k'_f r'_0).$$

Case 3: Two Elastic Spheres

$$\begin{bmatrix}
A^1_{n,1}(r'_1) & A^2_{n,1}(r'_1) & 0 & 0 & D^1_{n,1}(r'_1) & D^2_{n,1}(r'_1) & 0 & 0 & 0 \\
B^1_{n,1}(r'_1) & B^2_{n,1}(r'_1) & 0 & 0 & E^1_{n,1}(r'_1) & E^2_{n,1}(r'_1) & 0 & 0 & 0 \\
0 & 0 & C^1_{n,1}(r'_1) & C^2_{n,1}(r'_1) & 0 & 0 & 0 & 0 & 0 \\
A^1_{n,1}(r'_0) & A^2_{n,1}(r'_0) & 0 & 0 & D^1_{n,1}(r'_0) & D^2_{n,1}(r'_0) & -A^1_{n,0}(r'_0) & 0 & -D^1_{n,o}(r'_0) \\
B^1_{n,1}(r'_0) & B^2_{n,1}(r'_0) & 0 & 0 & E^1_{n,1}(r'_0) & E^2_{n,1}(r'_0) & -B^1_{n,0}(r'_0) & 0 & -E^1_{n,0}(r'_0) \\
0 & 0 & C^1_{n,1}(r'_0) & C^2_{n,1}(r'_0) & 0 & 0 & 0 & -C^1_{n,0}(r'_0) & 0 \\
\hat{A}^1_{n,1}(r'_0) & \hat{A}^2_{n,1}(r'_0) & 0 & 0 & \hat{D}^1_{n,1}(r'_0) & \hat{D}^2_{n,1}(r'_0) & -A^1_{n,0}(r'_0) & 0 & -\hat{D}^1_{n,0}(r'_0) \\
\hat{B}^1_{n,1}(r'_0) & \hat{B}^2_{n,1}(r'_0) & 0 & 0 & \hat{E}^1_{n,1}(r'_0) & \hat{E}^2_{n,1}(r'_0) & -\hat{B}^1_{n,0}(r'_0) & 0 & -\hat{E}^1_{n,0}(r'_0) \\
0 & 0 & \hat{C}^1_{n,1}(r'_0) & \hat{C}^2_{n,1}(r'_0) & 0 & 0 & 0 & -\hat{C}^1_{n,0}(r'_0) & 0
\end{bmatrix}
\begin{bmatrix}
\alpha^{m,1}_{n,1} \\ \alpha^{m,2}_{n,1} \\ \beta^{m,1}_{n,1} \\ \beta^{m,2}_{n,1} \\ \gamma^{m,1}_{n,1} \\ \gamma^{m,2}_{n,1} \\ \alpha^{m}_{n,0} \\ \beta^{m}_{n,0} \\ \gamma^{m}_{n,0}
\end{bmatrix} = \boldsymbol{0}$$

APPENDIX C:

$$A^l_{n,i}(r') = -\left[\frac{4\mu'_i}{r'}\dot{g}^l_n(k'_{p,i}r') + 2\mu'_i k'_{p,i}\left(1-\frac{n(n+1)}{k'^2_{p,i}r'^2}\right)g^l_n(k'_{p,i}r') + \lambda'_i k'_{p,i} g^l_n(k'_{p,i}r'))\right],$$

$$B^l_{n,i}(r') = 2\mu'_i\sqrt{n(n+1)}\left[\frac{1}{r'}\dot{g}^l_n(k'_{p,i}r') - \frac{g^l_n(k'_{p,i}r')}{k'_{p,i}r'^2}\right],$$

$$C^l_{n,i}(r') = \mu'_i\sqrt{n(n+1)}\left[k'_{s,i}\dot{g}^l_n(k'_{s,i}r') - \frac{1}{r'}g^l_n(k'_{s,i}r')\right],$$

$$D^l_{n,i}(r') = 2\mu'_i n(n+1)\left[\frac{\dot{g}^l_n(k'_{s,i}r')}{r'} - \frac{g^l_n(k'_{s,i}r')}{k'_{s,i}r'^2}\right],$$

$$E^l_{n,i}(r') = \mu'_i\sqrt{n(n+1)}\left[-2\frac{\dot{g}^l_n(k'_{s,i}r')}{r'} - k'_{s,i}g^l_n(k'_{s,i}r') + 2\frac{n(n+1)-1}{k'_{s,i}r'^2}g^l_n(k'_{s,i}r')\right],$$

and

$$\hat{A}^l_{n,i}(r') = \dot{g}^l_n(k'_{p,i}r'),$$

$$\hat{B}^l_{n,i}(r') = \sqrt{n(n+1)}\frac{g^l_n(k'_{p,i}r')}{k'_{p,i}r'},$$

$$\hat{C}^l_{n,i}(r') = \sqrt{n(n+1)}g^l_n(k'_{s,i}r'),$$

$$\hat{D}^l_{n,i}(r') = n(n+1)\frac{g^l_n(k'_{s,i}r')}{k'_{s,i}r'},$$

$$\hat{E}^l_{n,i}(r') = \sqrt{n(n+1)}\left[\dot{g}^l_n(k'_{s,i}r') + \frac{g^l_n(k'_{s,i}r')}{k'_{s,i}r'}\right].$$

Figure 2: Convergence of u_r as a function of time t for the FF - Model for $k' = 21,41,51$.
$(r = r_1,\ \theta = \pi/2,\ \varphi = \pi/2)$

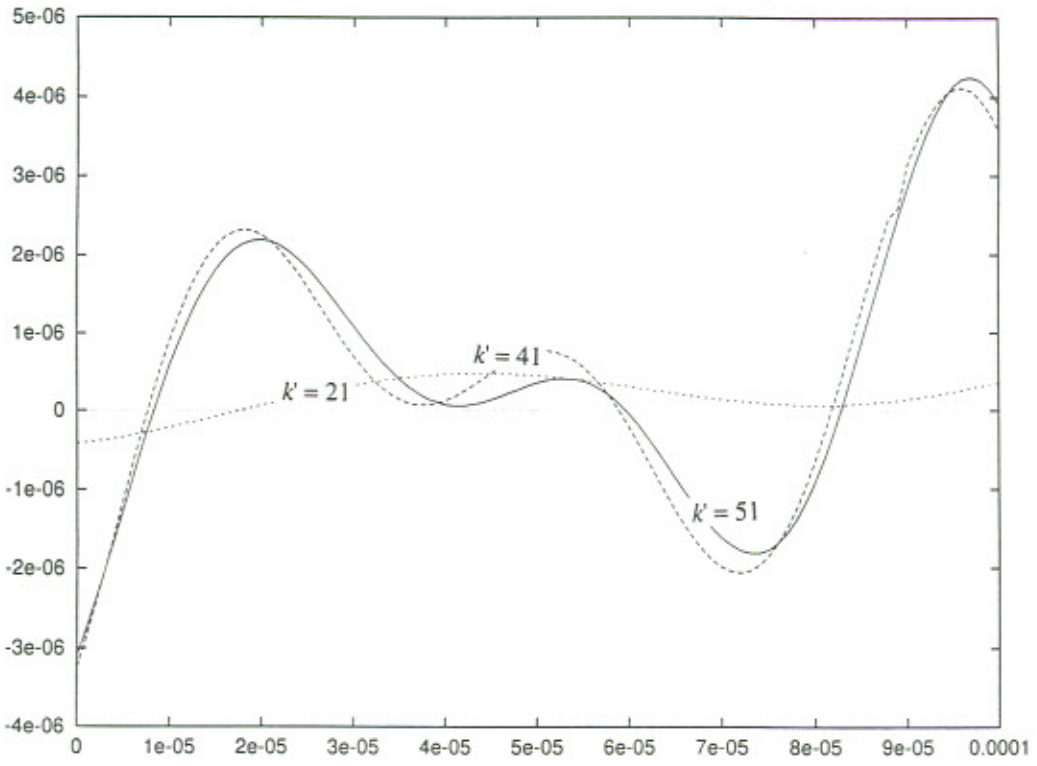

Figure 3: Displacements u_r, u_φ, u_θ as a function of time for the S - Model $(r = r_1,\ \varphi = \pi/2,\ \theta = 0)$.

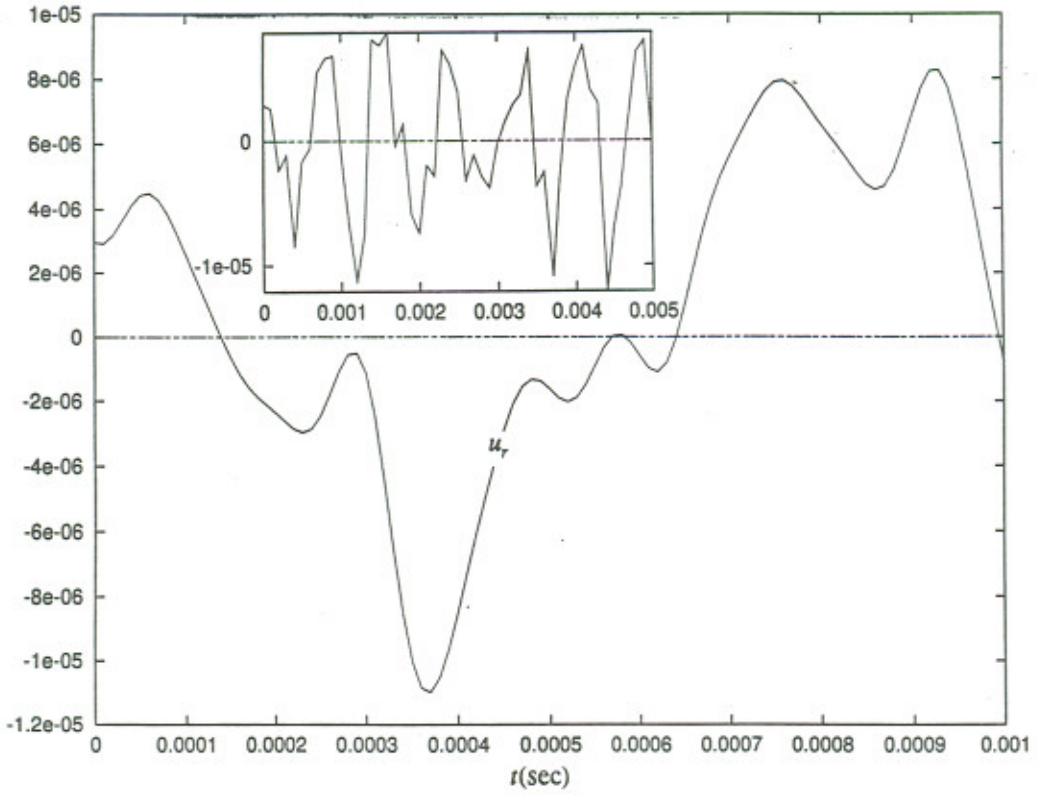

Figure 4: Displacements u_r, u_φ, u_θ as a function of time for the S- Model $(r = r_1,\ \varphi = \pi/2,\ \theta = \pi/2)$.

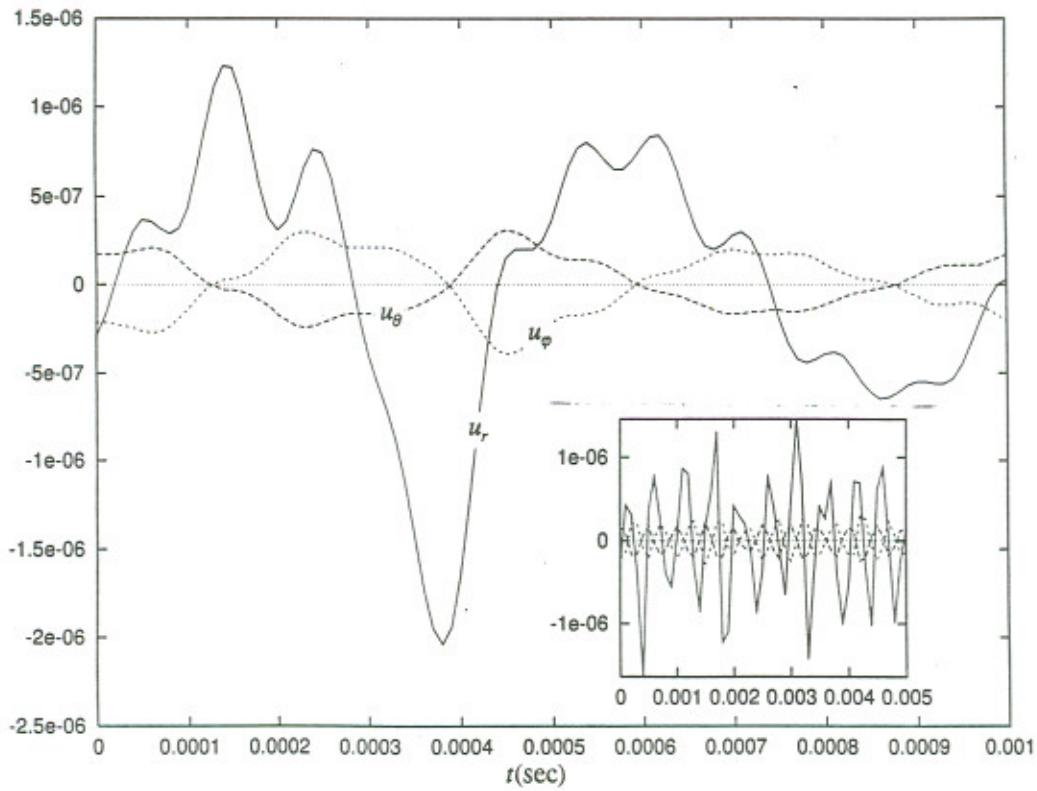

Figure 5: Displacements u_r, u_φ, u_θ for the S - Model for $r = r_1$
(A: $\theta = \pi$, $t = 0.0\,\text{sec}$, B: $\theta = \pi$, $t = 0.0004\,\text{sec}$, C: $\theta = \pi$, $t = 0.0008\,\text{sec}$,
D: $\theta = \pi/2$, $t = 0.0\,\text{sec}$, E: $\theta = \pi/2$, $t = 0.0003\,\text{sec}$, F: $\theta = \pi/2$, $t = 0.0008\,\text{sec}$).

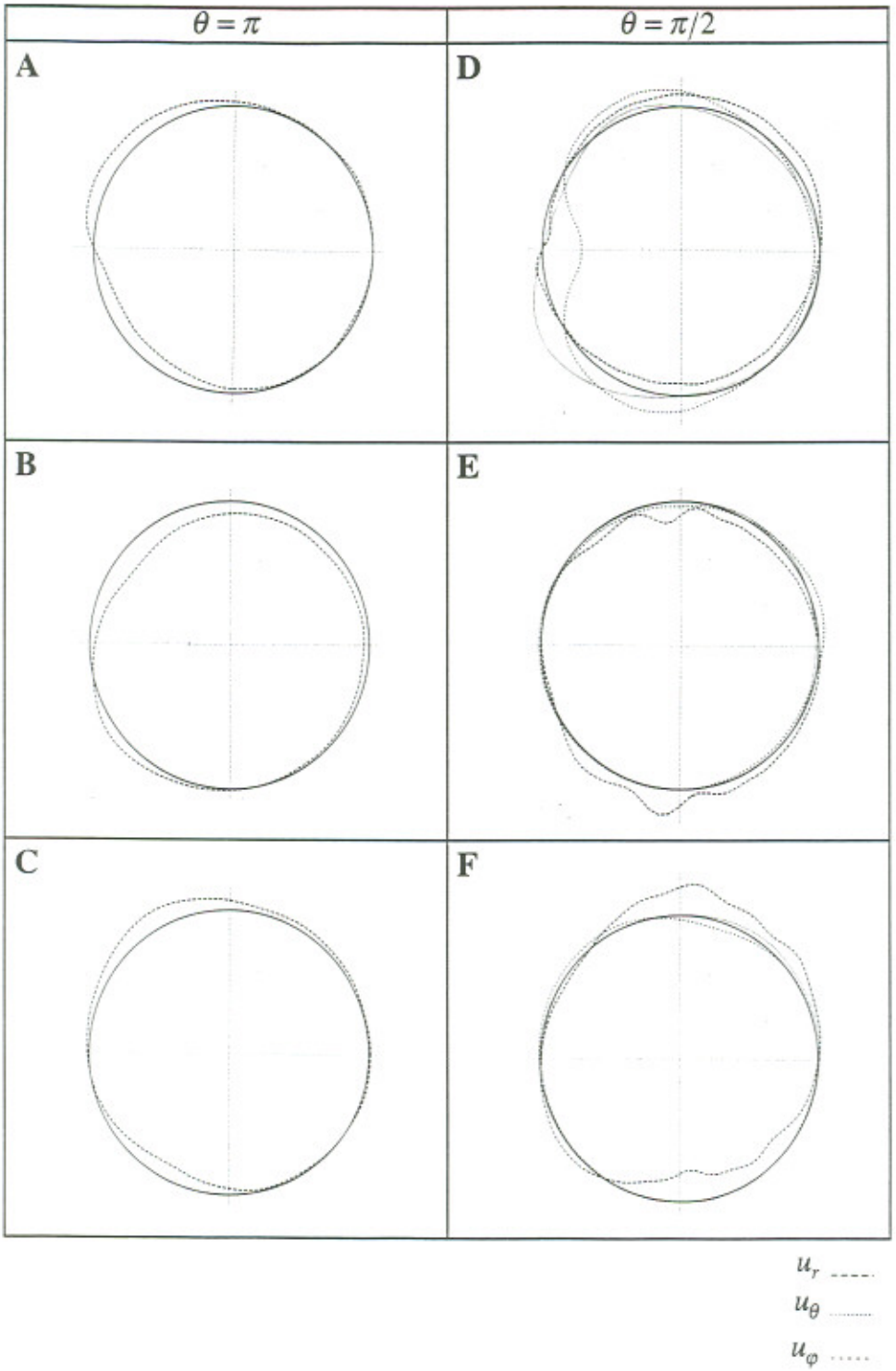

Figure 6: Displacements u_r, u_φ, u_θ as a function of time for the EE - Model $(r = r_1,\ \varphi = \pi/2,\ \theta = 0)$.

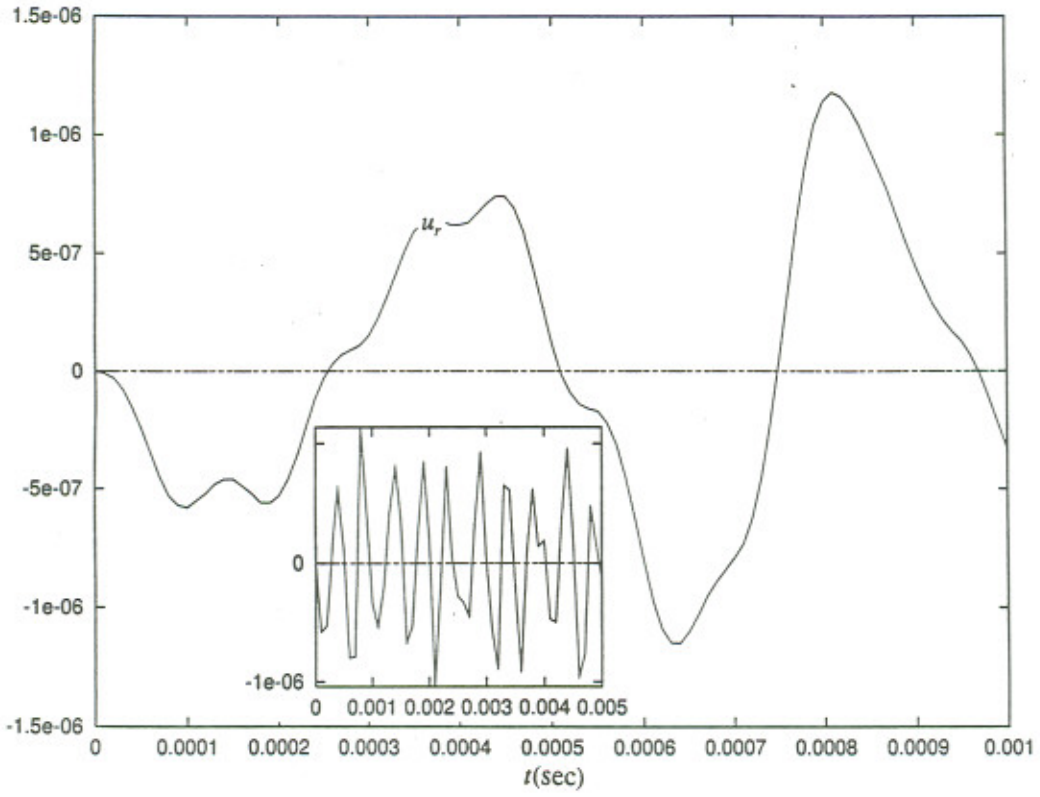

Figure 7: Displacements u_r, u_φ, u_θ as a function of time for the EE - Model $(r = r_1,\ \varphi = \pi/2,\ \theta = \pi/2)$.

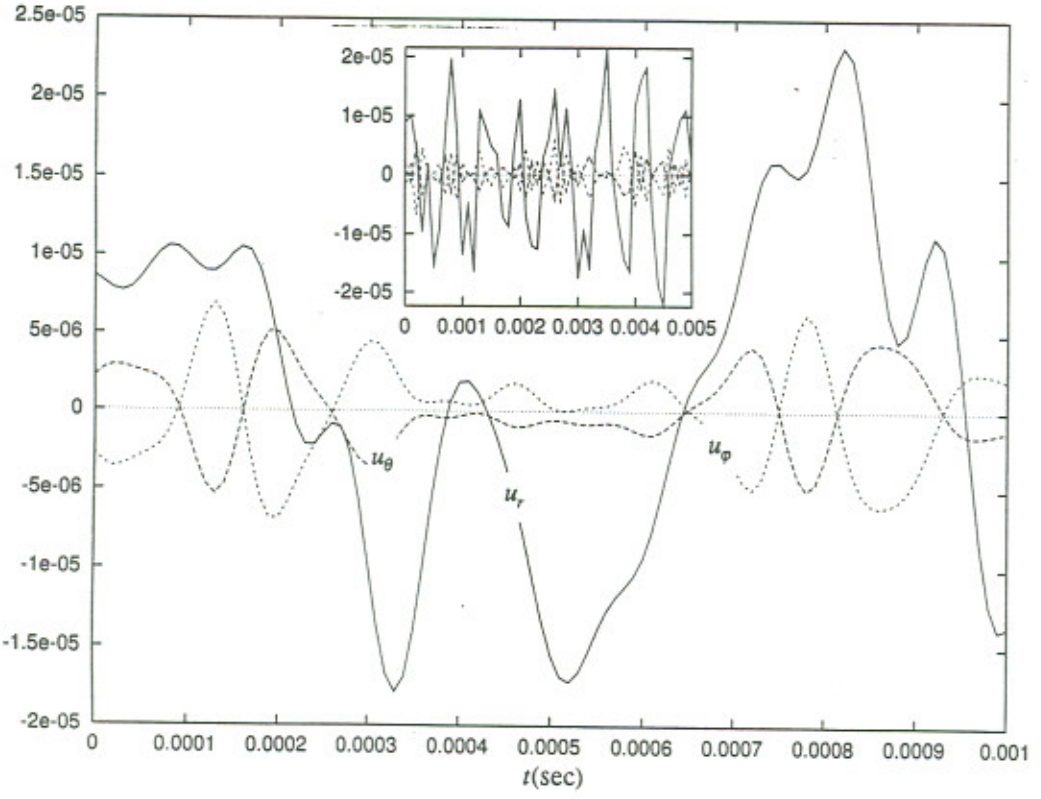

Figure 8: Displacements u_r, u_φ, u_θ for the EE - Model for $r = r_1$
(A: $\theta = \pi$, $t = 0.0002\,\text{sec}$, B: $\theta = \pi$, $t = 0.0004\,\text{sec}$, C: $\theta = \pi$, $t = 0.0006\,\text{sec}$,
D: $\theta = \pi/2$, $t = 0.0002\,\text{sec}$, E: $\theta = \pi/2$, $t = 0.0004\,\text{sec}$, F: $\theta = \pi/2$, $t = 0.0006\,\text{sec}$).

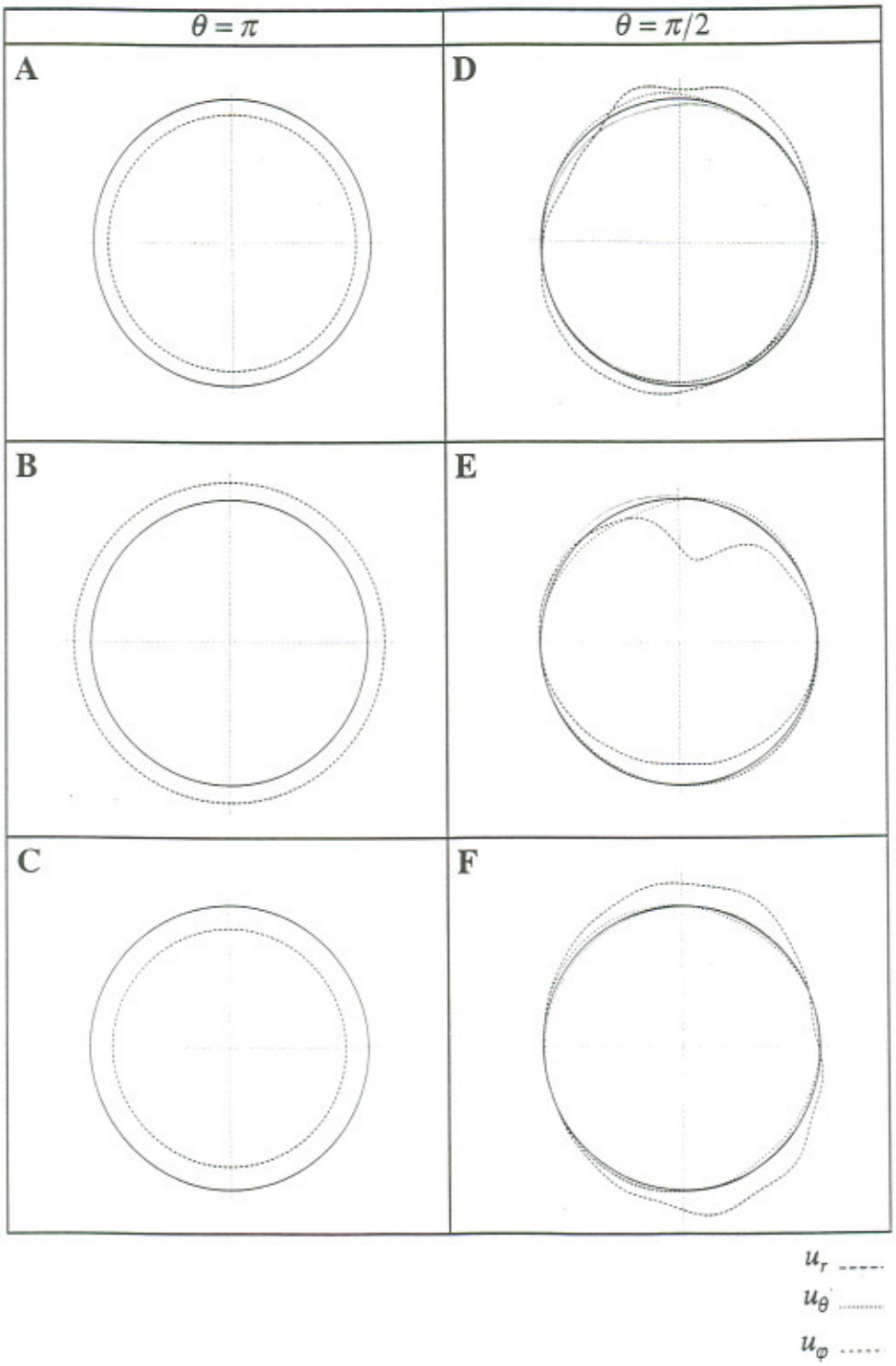

Figure 9: Displacements u_r, u_φ, u_θ as a function of time for the FF - Model $(r = r_1,\ \varphi = \pi/2,\ \theta = 0)$.

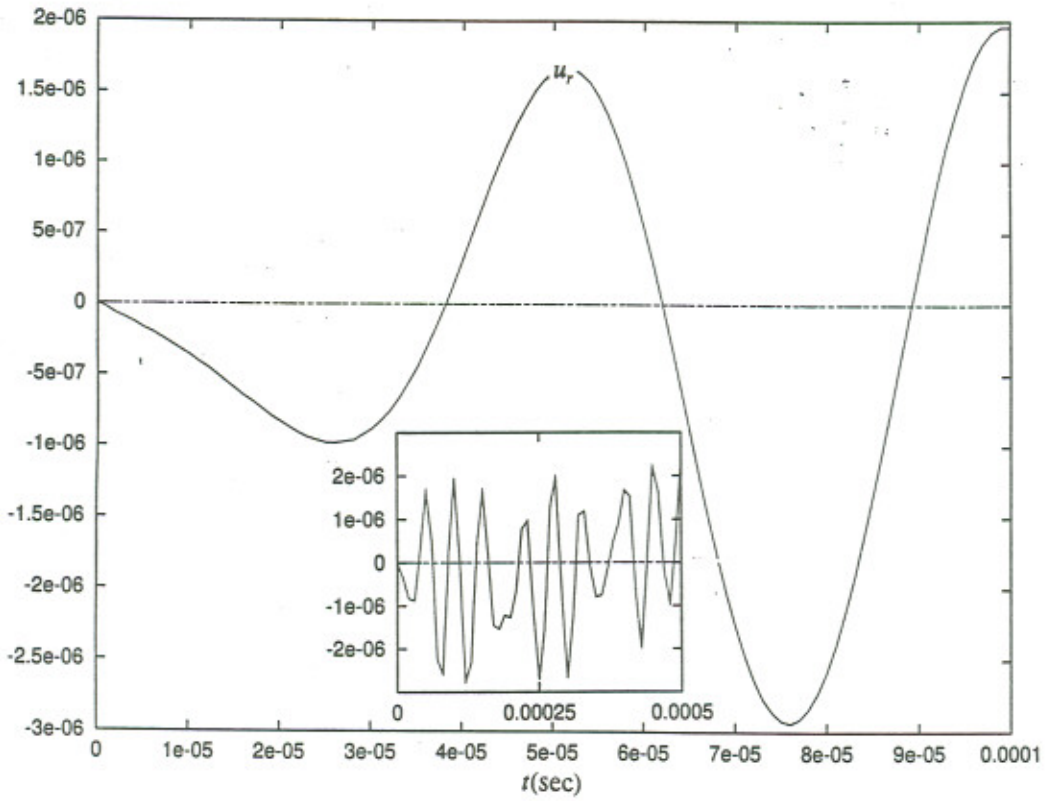

Figure 10: Displacements u_r, u_φ, u_θ as a function of time for the FF - Model $(r = r_1,\ \varphi = \pi/2,\ \theta = \pi/2)$.

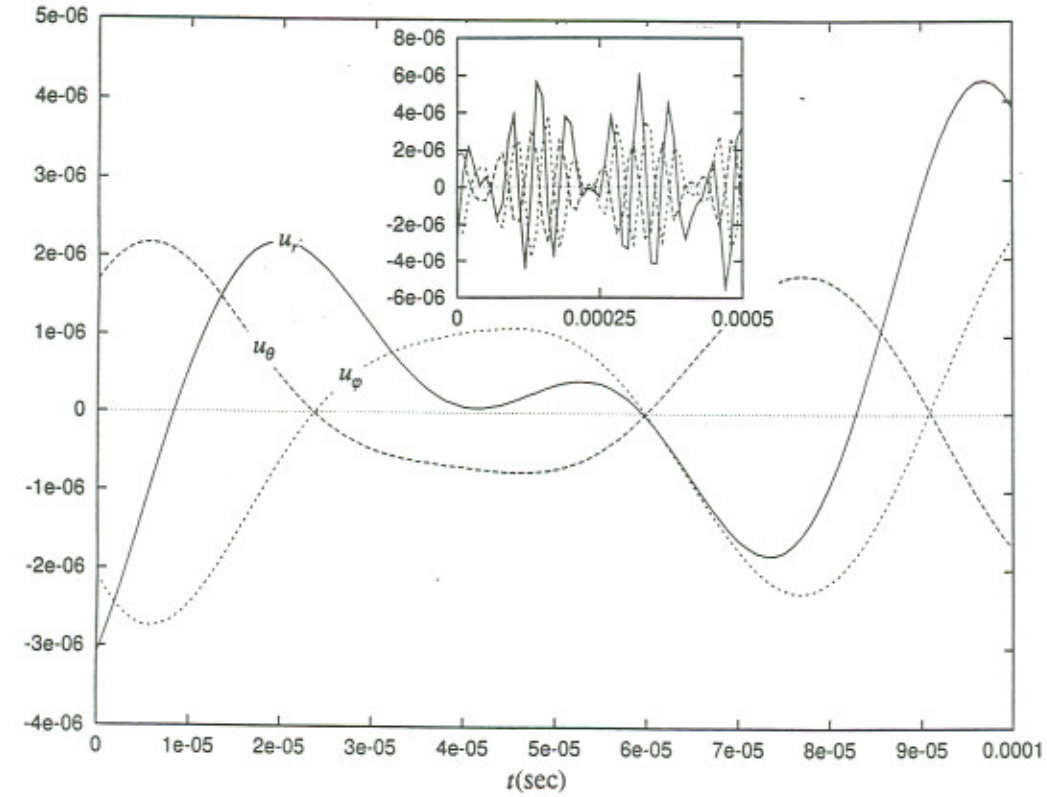

Figure 11: Displacements u_r, u_φ, u_θ for the FF - Model for $r = r_1$
(A: $\theta = \pi$, $t = 0.00002\,\text{sec}$, B: $\theta = \pi$, $t = 0.00004\,\text{sec}$, C: $\theta = \pi$, $t = 0.00008\,\text{sec}$,
D: $\theta = \pi/2$, $t = 0.00002\,\text{sec}$, E: $\theta = \pi/2$, $t = 0.00004\,\text{sec}$, F: $\theta = \pi/2$, $t = 0.00008\,\text{sec}$).

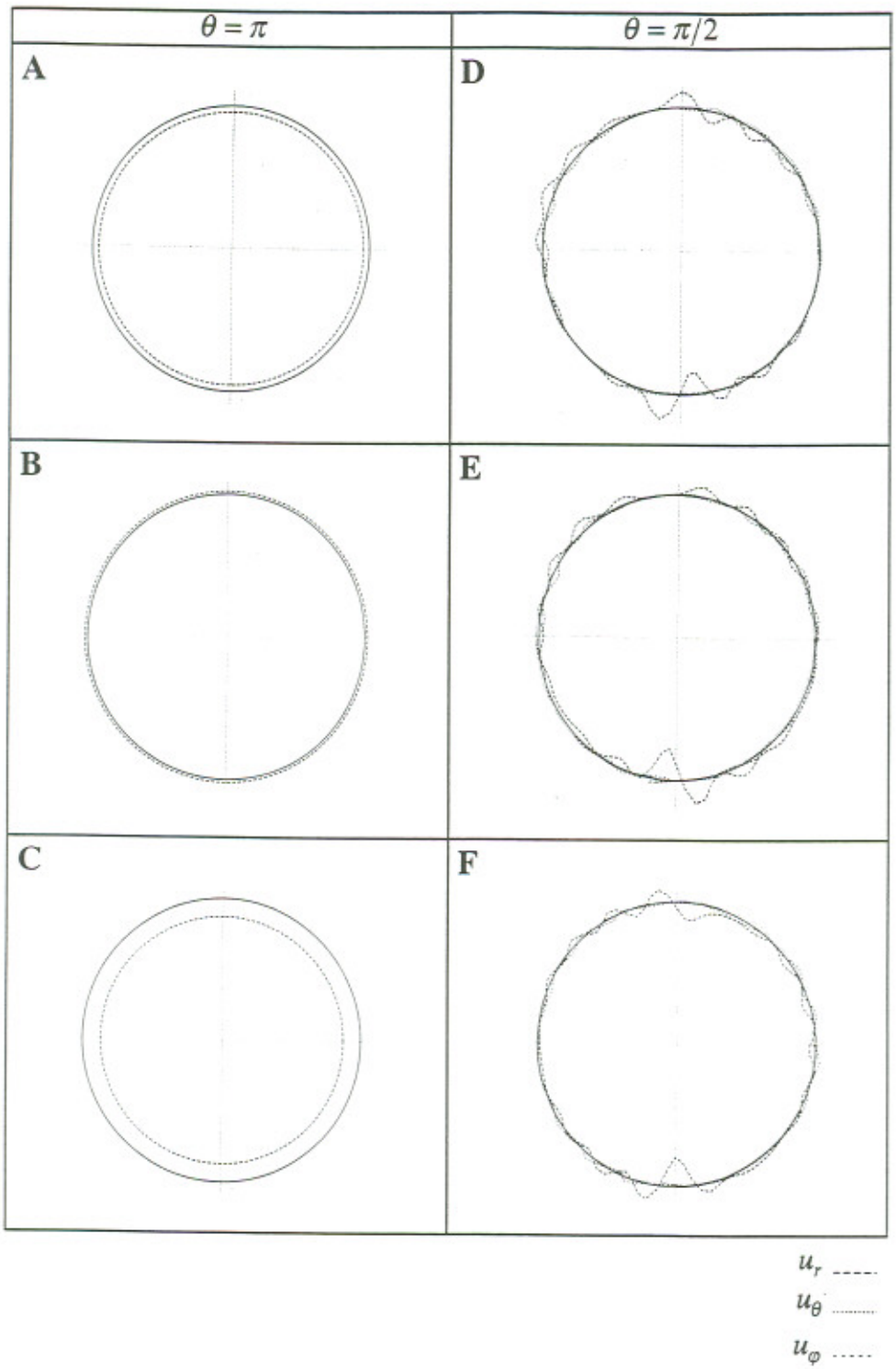

Figure 12: Pressure P as a function of time for the FF - Model
$(r = \frac{1}{2} r_0,\ \varphi = \pi/2,\ \theta = 0)$.

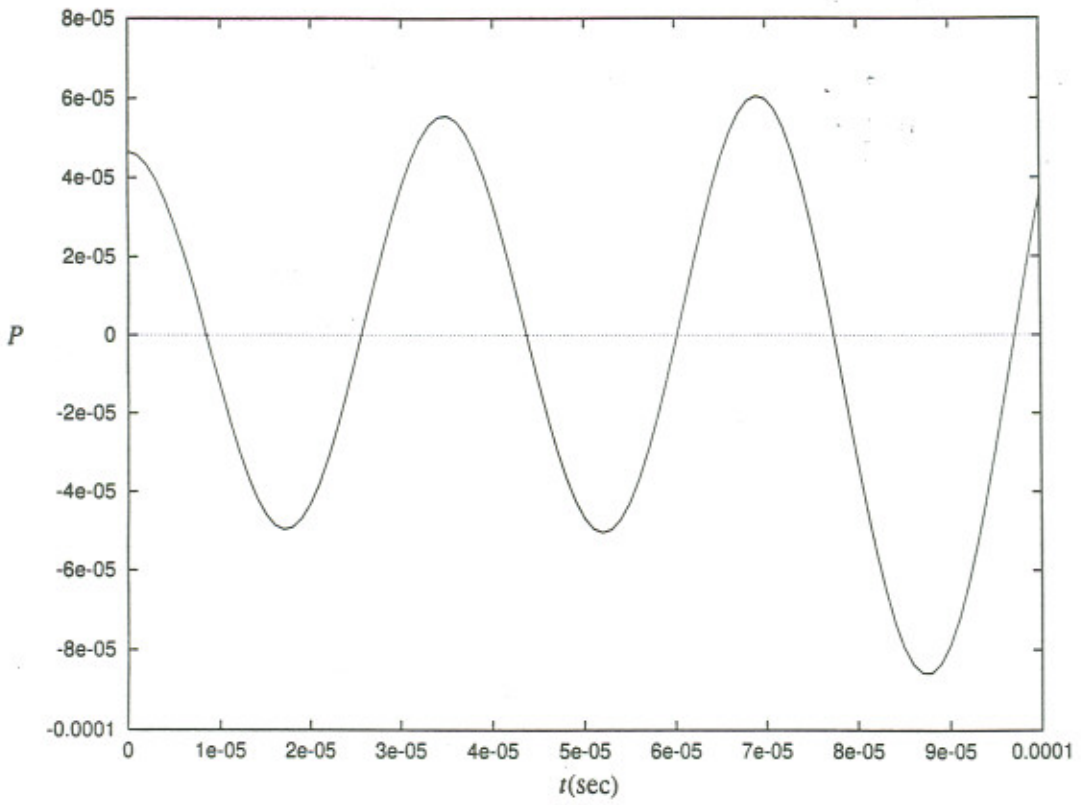

Figure 13: Pressure distribution for the FF - Model
$(0 \le r \le r_0,\ \varphi = \pi/2,\ \theta = \pi/2,\ t = 0.0001\text{sec})$.